AGU100 ADVANCING EARTH AND SPACE SCIENCE

JGR

Journal of Geophysical Research: Atmospheres

RESEARCH ARTICLE

10.1029/2017JD028166

Key Points:
- Multisite observations constrain California's annual N_2O emissions
- California's N_2O emissions are 1.5–2.5 times a recent state inventory
- Emissions are similar across seasons within posterior uncertainties

Supporting Information:
- Supporting Information S1

Correspondence to:
S. Jeong,
sjeong@lbl.gov

Citation:
Jeong, S., Newman, S., Zhang, J., Andrews, A. E., Bianco, L., Dlugokencky, E., et al. (2018). Inverse estimation of an annual cycle of California's nitrous oxide emissions. *Journal of Geophysical Research: Atmospheres*, *123*, 4758–4771. https://doi.org/10.1029/2017JD028166

Received 6 DEC 2017
Accepted 13 APR 2018
Accepted article online 25 APR 2018
Published online 7 MAY 2018

Inverse Estimation of an Annual Cycle of California's Nitrous Oxide Emissions

Seongeun Jeong[1], Sally Newman[2,3], Jingsong Zhang[4], Arlyn E. Andrews[5], Laura Bianco[5,6], Ed Dlugokencky[5], Justin Bagley[1], Xinguang Cui[1], Chad Priest[4], Mixtli Campos-Pineda[4], and Marc L. Fischer[1]

[1]Lawrence Berkeley National Laboratory, Berkeley, CA, USA, [2]California Institute of Technology, Pasadena, CA, USA, [3]Now at Bay Area Air Quality Management District, San Francisco, CA, USA, [4]Department of Chemistry and Air Pollution Research Center, University of California, Riverside, CA, USA, [5]Earth System Research Laboratory, NOAA, Boulder, CO, USA, [6]Cooperative Institute for Research In Environmental Sciences, University of Colorado Boulder, Boulder, CO, USA

Abstract Nitrous oxide (N_2O) is a potent long-lived greenhouse gas (GHG) and the strongest current emissions of global anthropogenic stratospheric ozone depletion weighted by its ozone depletion potential. In California, N_2O is the third largest contributor to the state's anthropogenic GHG emission inventory, though no study has quantified its statewide annual emissions through top-down inverse modeling. Here we present the first annual (2013–2014) statewide top-down estimates of anthropogenic N_2O emissions. Utilizing continuous N_2O observations from six sites across California in a hierarchical Bayesian inversion, we estimate that annual anthropogenic emissions are 1.5–2.5 times (at 95% confidence) the state inventory (41 Gg N_2O in 2014). Without mitigation, this estimate represents 4–7% of total GHG emissions assuming that other reported GHG emissions are reasonably correct. This suggests that control of N_2O could be an important component in meeting California's emission reduction goals of 40% and 80% below 1990 levels of the total GHG emissions (in CO_2 equivalent) by 2030 and 2050, respectively. Our seasonality analysis suggests that emissions are similar across seasons within posterior uncertainties. Future work is needed to provide source attribution for subregions and further characterization of seasonal variability.

1. Introduction

Nitrous oxide (N_2O) is the third most important long-lived greenhouse gas (GHG) behind carbon dioxide (CO_2) and methane (CH_4) (Hofmann et al., 2006; Montzka et al., 2011), in part due to its long atmospheric residence time (114 years; Solomon et al., 2007) and strong ability to absorb infrared radiation. The atmospheric N_2O burden has increased since the start of the industrial revolution. Also, N_2O is the dominant ozone-depleting gas species due to its large emission rate when weighted by its ozone depletion potential (Ravishankara et al., 2009). Although total N_2O emissions are significantly lower than CO_2 emissions, the global warming potential (radiative forcing integrated over 100 years) of N_2O is 298 times greater than that of CO_2 (California Air Resources Board, CARB, 2016; Myhre et al., 2013). Since 1750, the atmospheric concentration of N_2O has increased by approximately 20% at the global scale (United States Environmental Protection Agency, U.S. EPA, 2015).

N_2O is the third most important GHG in California after CH_4 (9% of the 2014 total GHG in Tg CO_2 equivalent (CO_2eq) using 100-year global warming potential) and CO_2 (84%). Anthropogenic sources in California's bottom-up inventory are estimated to emit approximately 41 Gg (10^9 g) N_2O/year, equivalent to about 3% of California's total GHG emissions when converted to CO_2eq (CARB, 2016). However, California's N_2O emissions have been underestimated in the bottom-up inventory (Jeong, Zhao, Andrews, Dlugokencky, et al., 2012; Xiang et al., 2013) and thus need to be further investigated. Also, N_2O can potentially be important as the state implements mitigations reducing sources of other GHG emissions. In California, quantitative accounting for N_2O and other GHGs is essential because California committed to an ambitious plan to reduce GHG emissions to 1990 levels of the total GHG emissions (in CO_2eq) by 2020 through Assembly Bill 32 (AB32, passed in 2006), which is the first binding policy to address climate change in the United States (Legislative Information, 2006). In 2016 California's legislature passed Senate Bill 32, which requires GHG emissions to be 40% below 1990 levels of the total GHG emissions (in CO_2eq) by 2030 (Legislative Information, 2016). Moreover, California's Executive Order S-3-05 establishes a GHG emission target of reducing state GHG emissions to 80% below 1990 levels by 2050 (Office of Governor, 2005). With clearly defined long-range goals for California's GHG emission reduction, it is essential to account for non-CO_2 emissions including N_2O to verify the implementation of the progressive targets.

Few studies, however, have attempted to assess California's N_2O emissions using atmospheric observations, while a number of studies (e.g., Cui et al., 2017; Jeong et al., 2013, 2016; Johnson et al., 2016; Wecht et al., 2014) have been conducted to estimate emissions for CH_4, which is another major non-CO_2 GHG regulated by law. Jeong, Zhao, Andrews, Dlugokencky, et al. (2012) estimated N_2O emissions in central California using 2 years of observations from a single tower and showed that actual N_2O emissions are significantly ($>$ 2 times) higher than the state inventory. Xiang et al. (2013) reported that the statewide emissions of N_2O during early summer (May–June) were 3–4 times higher than the Emission Database for Global Atmospheric Research (EDGAR) inventory and other inventories. These two studies are limited in constraining N_2O emissions due to lack of spatial or seasonal coverage, and California's annual N_2O emissions have not been fully evaluated.

Here we quantify both urban and rural N_2O emissions from California, presenting the first analysis of full annual N_2O emissions across California using atmospheric observations from six tower sites during June 2013 to May 2014. We use a hierarchical Bayesian inversion (HBI) method (Ganesan et al., 2014; Jeong et al., 2016, 2017), which allows us to assign probability distributions to the prior assumptions (e.g., uncertainty for the prior emissions) instead of using prescribed values. This study illustrates how uncertainty in inverse analysis can be treated by a combination of our best a priori knowledge of error sources (e.g., transport error) and statistical inference.

2. Materials and Methods

2.1. N_2O Measurements and Boundary Conditions

Dry-air N_2O mole fractions were measured at six tower sites across California (Table 1 and Figure 1). Among them, measurements from the Arvin (ARV), Sutter Buttes (STB), and Walnut Grove (WGC) sites mainly constrain emissions from California's Central Valley, while the Caltech (CIT), San Bernardino (SBC), and Sutro Tower (STR) sites are used to infer emissions from the major urban regions (South Coast Air Basin [SoCAB] and San Francisco Bay Area [SFBA]; see Figure 1 for site locations).

At most sites (except STR), the measurements are made using air sampling and analysis systems that combine pumps, membrane (Nafion) air driers, and calibrated gas analyzers. These sites utilized off-axis Integrated Cavity Output Spectroscopy (Los Gatos Research Inc. Model 907-0015), and air handling and calibration methods differed across the sites (Table 1). At a subset of sites (WGC, SBC) air sampling is switched between the multiple heights (WGC: 30, 91, and 483 m above ground level, every 300 s; SBC: 27 and 58 m above ground level, every 400 s) with measurements allowed to settle, with only the last 120 s used for the ambient air measurement. Only 91-m (WGC) and 58-m (SBC) measurements were used for the inverse model analysis. For other sites, measurements are made at a single height on those towers and switching was on only as was necessary for calibrations. N_2O measurements are averaged to 3-hr time intervals for inverse modeling with the exception of flask-air samples. As in previous work (e.g., Jeong, Zhao, Andrews, Dlugokencky, et al., 2012, Jeong et al., 2017, 2013), only daytime data are used in inverse modeling to reduce the impact of nighttime meteorology (e.g., nighttime boundary layer).

The uncertainty in the tower measurements are generated by a combination of short-term instrument noise (typically root-mean-square (RMS) value of 0.05 ppb for ~100-s average), atmospheric variability (typically $>$0.05 ppb and as large as 0.5 ppb for sites in regions with large N_2O emissions), and instrument offset drift relative to periodic calibration. As described below, the estimated accuracy of the calibration varied from approximately 0.2 ppb for well-calibrated sites (CIT, SBC, and WGC), 0.4 ppb for the site with only flask-air measurement (STR), to 1 ppb for the two valley sites with infrequent calibration (STB and ARV). The instrument offset and gain were measured periodically and corrected using two methods. For SBC and WGC, instruments were calibrated using three secondary gas standards tied to the WMO X2006A N_2O standard scale maintained at National Oceanic and Atmospheric Administration (NOAA; Hall et al., 2007). The offset and gain of the Los Gatos Research Inc. instrument were measured every 3 (WGC) and 4 hr (SBC) using two "high-low" secondary standards and then checked with the third "target" standard at times midway between the "high-

10.1029/2017JD028166

Table 1
GHG Site Information Across California

Site	Location	Latitude	Longitude	Inlet height (m, AGL)[a]	Measurement data availability	Instrument calibration comments
ARV[b]	Arvin	35.24	−118.79	10	October 2013 to May 2014	Precision check, 23 hr
CIT	Caltech, Pasadena	34.14	−118.12	10	June 2013 to May 2014	Offset calibration, 4.5 hr
STB[b]	Sutter Buttes	39.21	−121.82	10	April 2014 to May 2014	Precision check, 23 hr
STR	San Francisco	37.76	−122.45	232	June 2013 to May 2014	NOAA flasks, 2200 GMT
WGC	Walnut Grove	38.27	−121.49	91	June 2013 to May 2014	Offset and gain calibration + target check, 3 hr NOAA flasks 2200 GMT
SBC[b]	San Bernardino	34.09	−117.31	58	June 2013 to May 2014	Offset and gain calibration + target check, 4 hr

Note. AGL = above ground level; NOAA = National Oceanic and Atmospheric Administration.
[a]Inlet heights used in the inversion. Only 91-m (WGC) and 58-m (SBC) measurements were used for the inverse model analysis. For other sites, measurements were made at a single height on those towers and switching was on only as was necessary for calibrations. [b]Indicates California Air Resources Board's statewide greenhouse gas monitoring network sites.

low" calibrations. At CIT, offset and gain were calibrated every 3 months using NOAA primaries, and offset was calibrated using a secondary standard every 4.5 hr and checked for consistency using every other measurement. For the other two in situ sites (ARV and STB), a "precision check" was performed every 23 hr using an uncalibrated secondary gas cylinder of dry natural air. For two sites (WGC and STR), N_2O was measured in flask-air samples collected at 2200 GMT and analyzed by NOAA's cooperative air sampling network. For WGC, SBC, and CIT, target check measurements showed RMS variations less than 0.1 ppb. For WGC, the observed RMS difference between flask measurements and in situ measurements interpolated to the time of the flask sample varied from ~0.3 to 0.5 ppb, consistent with the repeatability of flask-air measurements (~0.3 ppb at 68% confidence). For sites with infrequent (23 hr) precision checks (ARV and STB), which do not facilitate correction of diurnal variations in instrument offset due to temperature, the observed RMS variation in the target checks was 0.5–1 ppb depending on time period. We note that the coastal site of Trinidad Head (THD) can be potentially useful for N_2O background in California. However, THD observations for our study period were not publicly available at the time of our analysis in 2015, which was conducted as part of a multigas project, and were not included in the inversion. In future studies, we will include THD data for N_2O background analysis when available.

The predicted N_2O upstream boundary values were estimated following the method used in Jeong, Zhao, Andrews, Dlugokencky, et al. (2012) and Jeong et al. (2013, 2016). As with previous work, N_2O boundary values were estimated using data from the Pacific coast N_2O vertical profiles (http://www.esrl.noaa.gov/gmd/ccgg/aircraft/) and remote Pacific marine boundary layer sampling sites (http://www.esrl.noaa.gov/gmd/ccgg/flask.html) within the NOAA Earth System Research Laboratory Cooperative Global Air Sampling Network. The data were smoothed and interpolated to create a three-dimensional (3-D) curtain, varying with latitude, height, and time. Following Jeong, Zhao, Andrews, Dlugokencky, et al. (2012) and Jeong et al. (2013), background uncertainty associated with the Pacific N_2O curtain was estimated by combining (in quadrature) the RMS error in the estimation of the 3-D curtain and the standard error of 500 Weather Research and Forecasting and Stochastic Time-Inverted Lagrangian Transport (WRF-STILT) background samples. The background uncertainties varied from 0.28 to 0.40 ppb depending on the site and season, which are similar to those (0.24–0.46 ppb) reported in Jeong, Zhao, Andrews, Dlugokencky, et al. (2012). The N_2O boundary values derived from the NOAA curtain showed biases during some seasons (mostly summer and spring). Xiang et al. (2013) also reported that the N_2O boundary values estimated from the NOAA curtain during May–June 2010 was systematically lower (1.6 ppb) compared to free tropospheric observations. The bias in the background was corrected together with other potential biases in measurements and transport while performing inversions (see section 2.4 and Text S2 for details on bias correction; Jeong et al., 2017).

2.2. Prior N_2O Emissions

We use the spatial distribution of EDGAR 42FT2010 (EDGAR, release version 4.2 Fast Track, http://edgar.jrc.ec.europa.eu; hereafter EDGAR) prior emission maps. The maps are then adjusted to conform to expectations for California by scaling EDGAR emissions to the CARB 2012 N_2O inventory (CARB, 2014). The CARB inventory does not include an estimate for personal product use, which is included in the industrial processes and

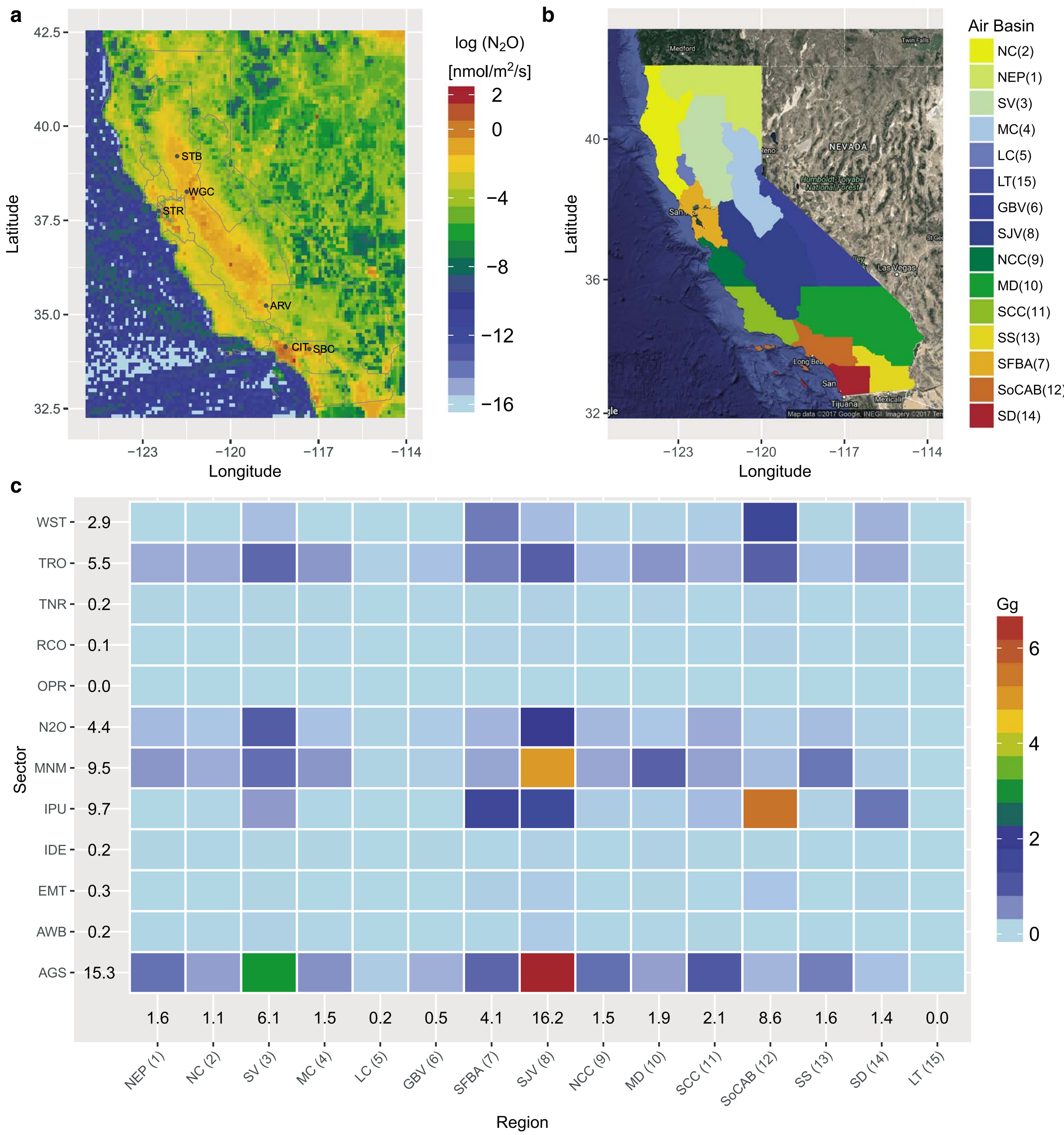

Figure 1. Prior N_2O emissions in California. (a) The total anthropogenic prior N_2O emissions used for inverse modeling (state total = 48.3 Gg N_2O/year) with locations of measurement sites across California, (b) region classification (California Air Basins, region numbers shown in the parentheses), and (c) emission summary (Gg N_2O/year) by region and sector. In (c), sectors include agricultural soils (AGS), manure management (MNM), agricultural waste burning (AWB), industrial processes and product use (IPU), energy manufacturing transformation (EMT), indirect emissions from NO_x and NH_3 (IDE), indirect N_2O emissions from agriculture (N2O), oil production and refineries (OPR), buildings (residential and others; RCO), waste (solid and wastewater; WST), nonroad transportation (TNR), and road transportation (TRO). Note that direct soil N_2O (AGS) is emitted from synthetic and manure fertilizers and crop residues left in the field while indirect N_2O emissions (N2O) are from nitrogen leaching and runoff. The numbers on the left and bottom of (c) represent emission sums by sector and region, respectively.

product use (IPU) sector of the EDGAR inventory. For the IPU sector, we use the estimate from EDGAR for inverse modeling, which accounts for 22% of the EDGAR total. The IPU sector in EDGAR includes emissions from chemical and solvents (e.g., nitric acid, adipic acid, and caprolactam; Janssens-Maenhout et al., 2014). Thus, the a priori emissions used here consist of a hybrid of emission estimates from the CARB and EDGAR N_2O inventories (state total = 48.3 Gg N_2O/year). In the prior model, emissions from both EDGAR and CARB are provided without temporal variation. Figure 1a shows the total (across sectors) prior anthropogenic emission map used in the inverse analysis. For region-specific analysis of N_2O, the total emissions are summed to subregions (Figure 1b) comprising California's Air Basins (http://www.arb.ca.gov/ei/maps/statemap/abmap.htm). In Figure 1c, we show a summary of the prior emissions (total = 48.3 Gg N_2O/year) used in the inversion. The Central Valley (Regions 3 and 8) emissions account for 46% of statewide total N_2O emissions and the two major urban regions (Regions 7 and 12) account for 26% of the total.

To estimate the contributions from natural environment, we consider N_2O emissions from natural soils and ocean. For the contributions from natural forest soils, we derive an emission map for natural forest based on the Global Emissions InitiAtive (GEIA) emission model (Bouwman et al., 1995) and include it in the inversion. Because the GEIA emissions are available at a coarse resolution of 1° × 1°, we used the Moderate Resolution Imaging Spectroradiometer land cover type data product (MCD12Q1, year 2012, available at http://e4ftl01.cr.usgs.gov/MOTA/MCD12Q1.051/2012.01.01/, accessed February 2015) to identify natural forest pixels at 0.1° (~10 km) resolution (see supporting information Figure S1). To minimize attribution of managed soils to natural forests, we included only the pixels with the forest area ratio (i.e., forest versus total area) greater than 80%. We note that the EDGAR model estimates nonzero anthropogenic N_2O emissions in most of California except for the desert area and part of the northern forest region. To generate 0.1° natural forest N_2O emissions, we assigned the 1° × 1° GEIA emissions from soils under natural vegetation and fertilized agricultural fields to the identified natural forest pixels based on the Moderate Resolution Imaging Spectroradiometer-derived natural forest map (supporting information Figure S2). The prior N_2O emission total from natural forest is 2.2 Gg N_2O/year, which is 4.6% of the state total anthropogenic N_2O emissions. Similarly, we used ocean N_2O emissions from the GEIA model (Bouwman et al., 1995) to incorporate emissions from the ocean along the California coast to the inversion system. The total ocean N_2O emission from the GEIA model within our entire modeling domain over the Pacific Ocean (see Figure S3) is 60 Gg N_2O/year.

2.3. Atmospheric Transport Modeling

We use the coupled WRF-STILT model for particle trajectory simulations (Lin et al., 2003; Nehrkorn et al., 2010; Skamarock et al., 2008). We adopt the setup used in Jeong et al. (2016) and Bagley et al. (2017) to run the STILT model (see supporting information Figure S4 for the WRF domain). In this setup, an ensemble of 500 STILT particles is run backward in time for 7 days driven with meteorology from the WRF model (version 3.5.1; Skamarock et al., 2008). The details for WRF model evaluation are described in Bagley et al. (2017) where transport errors are evaluated using meteorological observations and carbon monoxide (CO) for the same period as this study (June 2013 to May 2014). Here we briefly summarize the WRF simulations. We simulated meteorology for four different horizontal resolutions (vertical levels = 50) of 36, 12, 4, and 1.3 km (two inner domains for SFBA and SoCAB) using initial and boundary meteorological conditions provided by the North American Regional Reanalysis data set (Mesinger et al., 2006). For surface physics, we used two different land surface models (LSMs) depending on the location of each site (Bagley et al., 2017; Jeong et al., 2013, 2016; see Table S1 for details). For the Central Valley, we use the five-layer thermal diffusion LSM (5-L LSM) to account for irrigation in the land surface process during summer (Jeong et al., 2013) while using the Noah LSM (Chen & Dudhia, 2001) for other seasons. For the urban areas, we use the Noah LSM for all seasons following Newman et al. (2013).

We use different planetary boundary layer (PBL) schemes depending on the location of GHG measurement sites (see Table S1). As a default for urban areas, we use the MYNN2 (Mellor-Yamada-Nakanishi-Niino level 2.5) PBL scheme (Nakanishi & Niino, 2006) coupled with the Noah LSM. For the Central Valley we also use the MYNN2 PBL scheme except for summer for which we use the MYJ (Mellor-Yamada-Janjić) scheme (Janjić, 1990; Mellor & Yamada, 1982) coupled with the 5-L LSM (Jeong et al., 2013, 2016). Based on the transport evaluation using predicted and measured CO data (Bagley et al., 2017), we apply the YSU (Yonsei University) PBL scheme (Hong et al., 2006) for a few cases (e.g., winter season in the southern San Joaquin Valley) to use an improved representation of topographic influences on boundary layer meteorology (Jiménez & Dudhia, 2012).

2.4. HBI

We use a HBI method (Ganesan et al., 2014; Jeong et al., 2016, 2017) to estimate regional N_2O emissions in California. We apply the following linear model to estimate scaling factors for adjusting prior emissions (Fischer et al., 2017; Jeong et al., 2013, 2016, 2017; Wecht et al., 2014; Zhao et al., 2009):

$$\mathbf{y} = \mathbf{K}\lambda + \mathbf{D} + \mathbf{v} \tag{1}$$

where $\mathbf{y}$ is the measurement vector ($n \times 1$), which represents mole fraction time series after subtracting background values, $\mathbf{K} = \mathbf{FE}$ (an $n \times k$ matrix), $\mathbf{F}$ is the footprint (sensitivity of concentration to changes in surface emission fluxes, $n \times m$), $\mathbf{E}$ is the prior emission flux ($m \times k$), λ is a $k \times 1$ vector for scaling factors with a covariance matrix $\mathbf{Q}$ ($k \times k$), and $\mathbf{v}$ is a vector representing the model-measurement mismatch with a covariance matrix $\mathbf{R}$ ($n \times n$, see Text S1 for the structure of $\mathbf{R}$). $\mathbf{D}$ is a vector for mean bias adjustments, which is simultaneously estimated with other parameters during the hierarchical inverse process. As demonstrated by Jeong et al. (2017), each element of the vector $\mathbf{D}$ (estimated for each month) represents a combination of mean background adjustments, measurement offsets, transport biases, and other potential biases for each site (see Text S2 for details; Jeong et al., 2017). To construct the final measurement and prediction data set used for equation (1), we applied similar data filtering methods based on well-mixed conditions and background sampling (Jeong, Zhao, Andrews, Bianco, et al., 2012; Jeong, Zhao, Andrews, Dlugokencky, et al., 2012; Jeong et al., 2013, 2016; see Figure S8 for data used in the inversion). Additional data filtering was performed based on fire periods and the CO analysis from Bagley et al. (2017). Bagley et al. (2017) showed that for some cases (e.g., winter in the southern San Joaquin Valley) WRF-STILT simulations could not capture temporal variations of CO well, underpredicting CO mole fractions relative to measurements. As in Jeong et al. (2016), we excluded data points for those hours identified by Bagley et al. (2017) from the inversion. We perform inversions for each month during the study period and solve for 197 values of λ in each month which include 183 pixels (at 0.3° × 0.3°) for the major regions (i.e., Regions 3, 7, 8, and 12 in Figure 1b), 11 nonmajor regions inside California, outside California for nonocean anthropogenic emissions, natural forest, and ocean regions. To implement this inversion scheme, the original prior predictions (i.e., $\mathbf{K}$ matrix) at 0.1° were aggregated into 0.3° pixels and regions (shown in Figure 1b) for the major and nonmajor regions, respectively (Jeong et al., 2016, 2017).

For the model in Equation (1), the joint parameter set we need to estimate is

$$\boldsymbol{\Theta} = \{\boldsymbol{\lambda}, \boldsymbol{\mu}_{\lambda}, \boldsymbol{\sigma}_{\lambda}, \boldsymbol{\sigma}_{\boldsymbol{R}}, \eta, \tau, \boldsymbol{D}\} \tag{2}$$

where λ is the scaling factor (for emission adjustments), $\boldsymbol{\mu}_{\lambda}$ is the prior mean for λ, $\boldsymbol{\sigma}_{\lambda}$ is the uncertainty for λ (i.e., square root of diagonal elements of $\mathbf{Q}$), and $\boldsymbol{\sigma}_{\mathbf{R}}$, η, and τ are the parameters used to construct the model-measurement mismatch covariance matrix $\mathbf{R}$ (see supporting information Text S1 for the representation of $\mathbf{R}$). In HBI we estimate the joint parameter set simultaneously, using the measurements only once (Ganesan et al., 2014; Jeong et al., 2016, 2017). Figure 2 shows the summary of the model-measurement mismatch uncertainties (diagonal terms of the $\mathbf{R}$ matrix) estimated for each month using the HBI method. The prior values shown in Figure 2 are derived based on the results from Jeong, Zhao, Andrews, Dlugokencky, et al. (2012) where they report the model-measurement uncertainty for the WGC site. Note that we need this prior value (as a hyperparameter) to construct a probability distribution from which we sample to estimate posterior values. For the WGC prior values, we adopt the estimates for $\mathbf{R}$ reported in Jeong, Zhao, Andrews, Dlugokencky, et al. (2012), and the prior values for the other sites are assumed to be proportional to the background-subtracted mean mole fraction relative to that of WGC (see Text S1 for details). The posterior uncertainty values (sampled from the posterior distribution) are generally similar to the prior values with a few exceptions. The results in Figure 2 show that the data used in the inversion is able to adjust our prior knowledge of the model-measurement uncertainty yielding values different from the prior estimates. Similarly, we estimated the diagonal terms of the $\mathbf{Q}$ matrix while performing the inversion and the results are presented in supporting information Figure S9.

With the parameter set identified, the posterior probability can be written as follows:

$$p(\boldsymbol{\lambda}, \boldsymbol{\mu}_{\lambda}, \boldsymbol{\sigma}_{\lambda}, \boldsymbol{\sigma}_{\boldsymbol{R}}, \eta, \tau, \boldsymbol{D}|\boldsymbol{y}) \propto p(\boldsymbol{y}|\lambda, \boldsymbol{\sigma}_{\boldsymbol{R}}, \eta, \tau, \mathbf{D}) p(\lambda|\boldsymbol{\mu}_{\lambda}, \boldsymbol{\sigma}_{\lambda}) p(\boldsymbol{\mu}_{\lambda}) p(\boldsymbol{\sigma}_{\lambda}) p(\boldsymbol{\sigma}_{\boldsymbol{R}}) p(\eta) p(\tau) p(\mathbf{D}) \tag{3}$$

where the right-hand side shows the likelihood function (i.e., the term that includes measurements $\mathbf{y}$) and the prior distribution for each parameter. Note that in equation (3) all variables are in vector form except for η and τ. Following Jeong et al. (2016), we use the Just Another Gibbs Sampler system (Plummer, 2003) and the R statistical language (https://cran.r-project.org/) to build Markov chain Monte Carlo (MCMC) samplers for the posterior distribution in equation (3). The individual probability distributions in equation (3) are described in supporting information Text S1 and convergence and accuracy of MCMC samples (50,000 samples for each

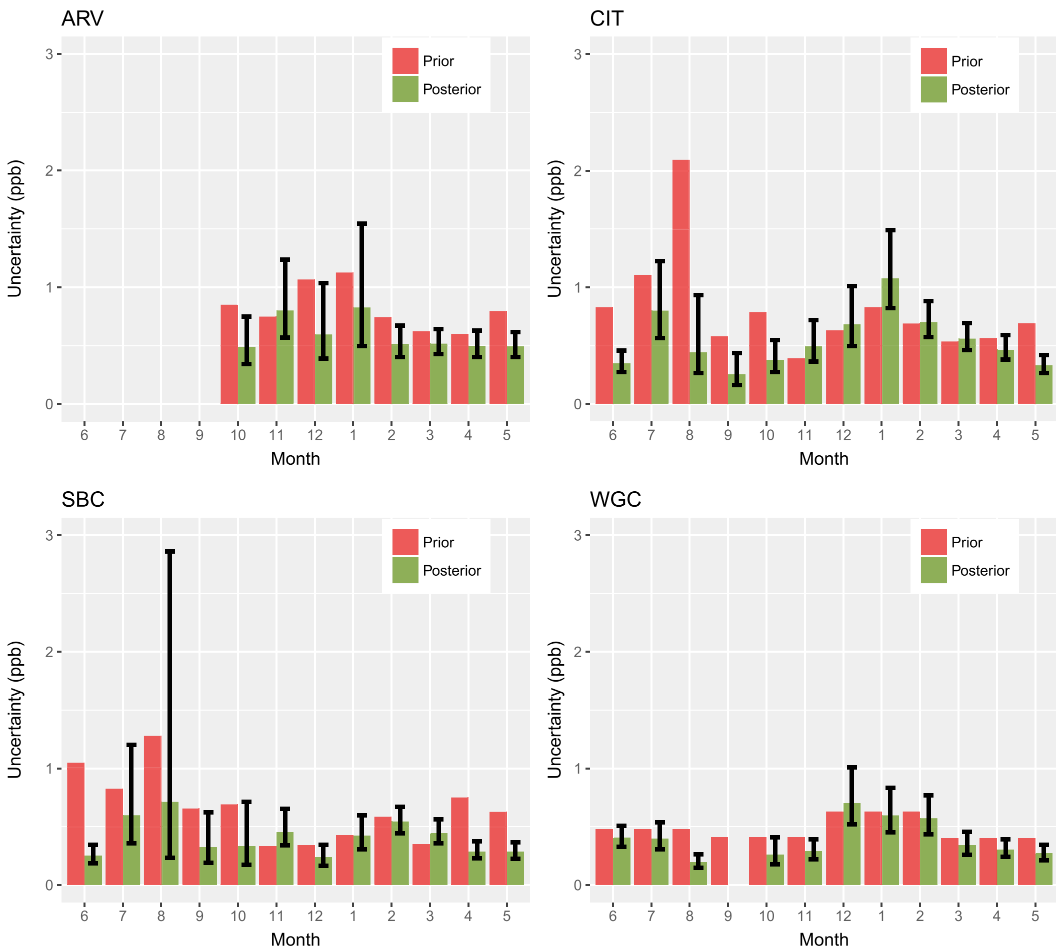

Figure 2. Estimated monthly model-measurement mismatch uncertainties at four major sites with continuous measurements during most of the study period (June 2013 to May 2014). The posterior values were estimated using 50,000 Markov chain Monte Carlo samples and the error bars represent the 95% confidence intervals (2σ). The uncertainty value for September at WGC was not estimated because most of the measurements were missing during the month.

parameter) are described in Text S3 (Gelman et al., 2014; Gelman & Hill, 2007; Gelman & Rubin, 1992; Kass et al., 1998; Korner-Nievergelt et al., 2015; Kruschke, 2015; Michalak, 2008; Miller et al., 2014; Rasmussen & Williams, 2006).

3. Results and Discussion

3.1. State Total Emissions

Regional anthropogenic N_2O emissions were estimated by multiplying the CARB-scaled EDGAR prior emissions (Figure 1a) by optimized scaling factors for emission adjustments. We estimated a scaling factor for each 0.3° pixel (total = 183 pixels) within the major emission regions (i.e., Regions 3, 7, 8, and 12 in Figure 1b), which account for 72% of the total prior emission. For the other 11 regions, we estimated a single scaling factor for each region (Jeong et al., 2013, 2016, 2017). Posterior emissions were estimated for both natural forest and ocean sources (see supporting information Figure S5), but those emissions were excluded from comparison to the CARB inventory, which includes anthropogenic emissions only. We note that the fractions of monthly mean predicted mole fractions for ocean and forest are less than ~10% of the total predicted mole fraction both before and after inversion at all sites with the exception of the Sutro coastal site (supporting information Figure S5). This small fraction of ocean mole fraction relative to the total agrees with the finding in Xiang et al. (2013), who reported only 0.2- to 0.3-ppb enhancements were explained by the ocean along California's coast during early summer of 2010. We note that, although the total ocean emission from the prior emission map is comparable to the state total emission, ocean emissions are weighted by the

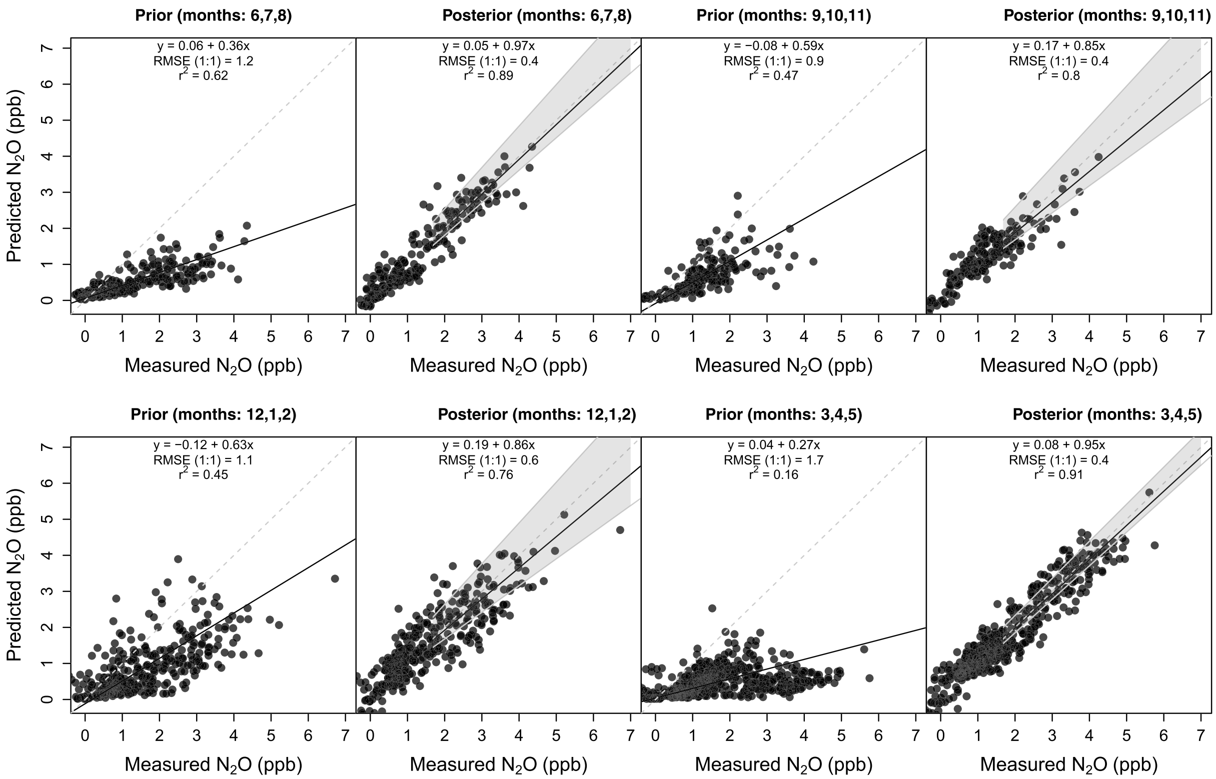

Figure 3. Comparison of predicted and measured N_2O mole fractions before (prior, bias not corrected) and after (posterior, bias corrected) inversion for each season. Note that, as shown in equation (3), the prediction in the posterior comparison represents mole fractions that were generated from a combination of optimized emissions and bias corrections. The gray dashed line is the 1:1 line and the black solid line indicates the best fit slope for the data (filled circles). For the posterior plot, the best fit slope was derived from the median values of the posterior emissions (i.e., 50,000 Markov chain Monte Carlo [MCMC] samples). The regression coefficients in the posterior plot were calculated based on the median values of the 50,000 MCMC samples. The gray shaded area in the posterior plot represents the 95% uncertainty region based on the upper and lower bounds of the 50,000 posterior MCMC samples.

weak footprint in the ocean (as compared to those on land), yielding generally less than 10% of the total mole fractions at most sites. This suggests that anthropogenic emissions are dominant sources of N_2O in California, as assumed by previous studies (Jeong, Zhao, Andrews, Dlugokencky, et al., 2012; Kort et al., 2008). Figure 3 shows regression analysis results between predicted and background-subtracted, measured mole fractions using all data used in the inversion for each season. The regression analysis was conducted using the lmodel2 package available from the R statistical language (https://cran.r-project.org/), which considers errors in both *x* and *y* axes. This simple analysis without full consideration of errors suggests that N_2O emissions are underestimated by the prior inventory model. After inversion, RMS error (RMSE) and coefficient of determination (r^2, prior = 0.16–0.62; posterior = 0.76–0.91) are significantly improved for all seasons. To test the difference between prior and posterior comparisons, we performed the Kruskal-Wallis rank sum test, which is similar to one-way analysis of variance but does not require normality of the data. The test result indicates that the posterior is different (i.e., improved) from the prior, showing $p < 0.05$ at a significance level of $\alpha = 0.05$.

The HBI analysis estimates the state total annual anthropogenic emissions are 62–101 Gg N_2O/year (median = 79 Gg, at 95% confidence). The median emission estimates for individual regions are shown in Figure 4a. The posterior state total emissions are 1.3–2.1 times larger than the prior total used in inverse modeling (i.e., a hybrid inventory that estimates emissions at 48 Gg N_2O/year, Figure 1; see Figure 4b for the posterior to prior ratio) and 1.5–2.5 times larger than the recent CARB inventory (41 Gg N_2O/year for 2014). This result is generally consistent with that of Jeong, Zhao, Andrews, Dlugokencky, et al. (2012) where their annual N_2O emission estimates for central California during 2008–2009 were 2 times the state inventory. The spatial distribution of anthropogenic emissions in Figure 4c shows that the major urban regions (SFBA and SoCAB) as well as the Central Valley are well constrained relative to the other regions. This is a

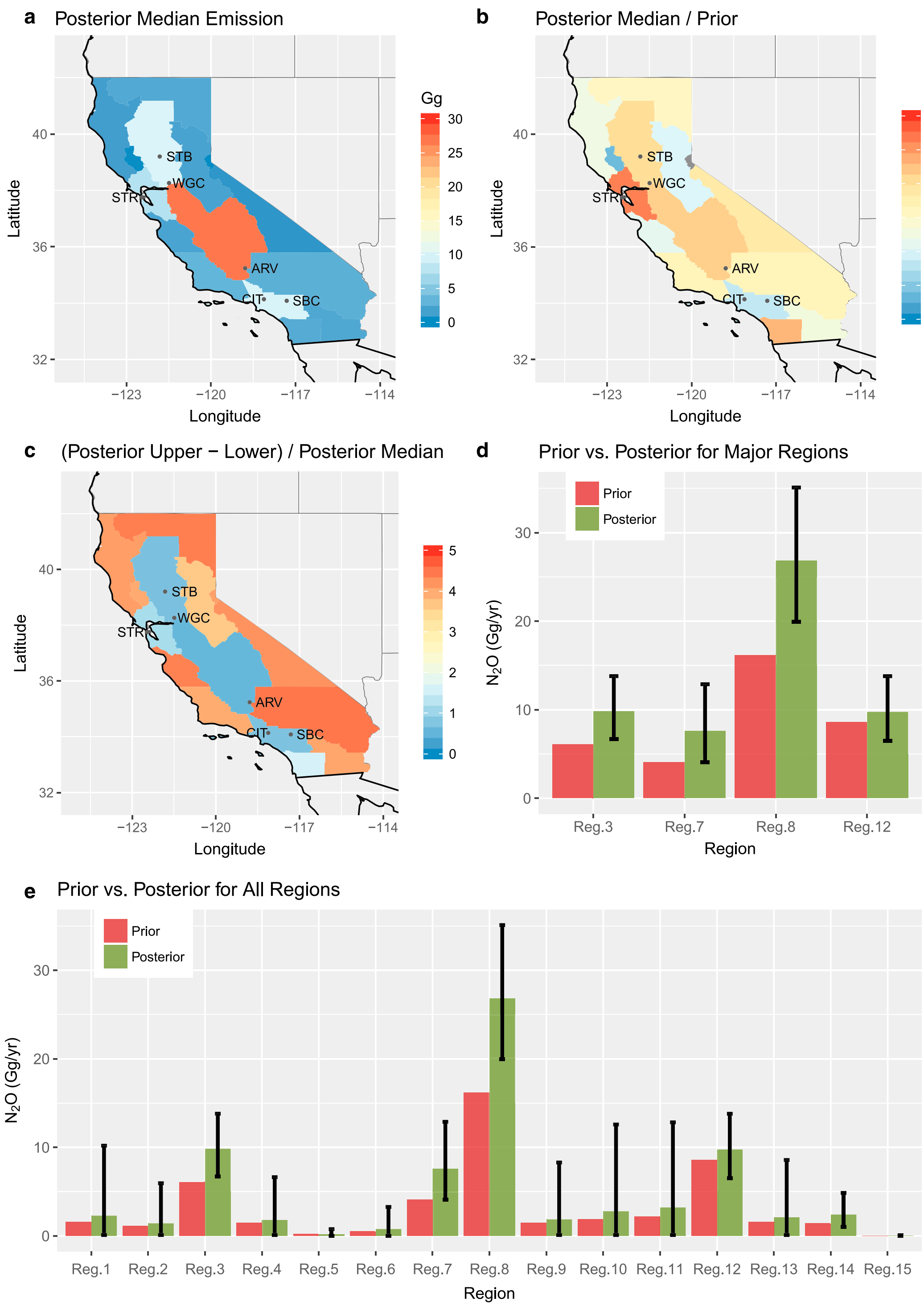

Figure 4. Comparison of anthropogenic annual prior and posterior emissions by region. (a) posterior (median) annual emissions (Gg N_2O/year), (b) ratio of the posterior median to prior, (c) ratio of the estimated 97.5th minus 2.5th percentile to prior, (d) estimated annual anthropogenic N_2O emissions for the major emission regions (at 95% confidence), and (e) estimated annual anthropogenic N_2O emissions for all regions. The major regions of 3, 7, 8, and 12 represent the Sacramento Valley (SV), San Francisco Bay Area (SFBA), San Joaquin Valley (SJV), and South Coast Air Basin (SoCAB), respectively.

significant improvement compared to the result from Jeong, Zhao, Andrews, Dlugokencky, et al. (2012) that used measurements from a single tower (WGC) located in central California. In this study, using pixel-based inversion we have significantly reduced the anticorrelation (<20%) in the posterior emissions for the major emitting regions (e.g., between Regions 3 and 7), compared to those (up to 60% depending on the season) of Jeong, Zhao, Andrews, Dlugokencky, et al. (2012; supporting information Figure S7). This indicates that our total emission for each sub-region is much more independent than those of the previous study.

3.2. Emissions From Major Rural and Urban Regions

The HBI using multiple sites across California constrains N_2O emissions from a significant portion of emission sources in both rural and urban regions of California. Figure 4d shows the summary for annual anthropogenic emissions for the major N_2O-emitting (72% of the total) regions in California constrained by measurements from our six towers (see Figure 4e for all regions). We first examine the emissions for rural regions of California, focusing on the Central Valley. We estimate that the Central Valley (Regions 3 and 8) emissions are 29.1–46.1 Gg N_2O/year (at 95% confidence). This result suggests that the inferred posterior emissions are larger than the prior total emission (22.3 Gg N_2O/year) for the Central Valley by factors of 1.3–2.1. This further suggests that the Central Valley is the major emitting region for California's N_2O emissions representing 37–58% of the posterior median (79 Gg), similar to that (46%) in the prior model.

For urban N_2O emissions of California, we consider emissions from the two major urban regions (SoCAB and SFBA). These urban regions account for 26% of the state's total N_2O emission according to the prior emission model. The HBI analysis estimates a total of 6.5–13.8 Gg N_2O/year for SoCAB (at 95% confidence), which is 0.8–1.6 times the prior. Similarly, we estimate the SFBA N_2O emissions to be 4.1–12.9 Gg N_2O/year, 1.0–3.1 times the prior. Combining posterior MCMC samples for the two major urban regions, we estimate the posterior emissions for the two regions to be 12.3–23.9 Gg N_2O/year (at 95% confidence), which are larger than the prior by factors of 1.0–1.9. Since the spatially explicit EDGAR prior emissions were scaled to CARB's inventory by source sector (see section 2.2), comparison with CARB's inventory for the urban regions requires an assumption about the spatial distribution of N_2O emissions. However, Xiang et al. (2013) suggested that the EDGAR inventory does not appear to provide good spatial representation of surface emissions in California. To resolve this potential source of error in the inversion, we first scaled the EDGAR emissions to match CARB's inventory by sector. We then conducted pixel-based inversions using large uncertainty (>100% for most pixels, see Figure S9) to allow for adjustment of potentially misrepresented emissions with more flexibility. When the inversion was performed at the pixel scale combined with flexible treatment of prior uncertainty, posterior predictions agreed well with measurements, and the posterior yields much higher correlations than those of the prior (see Figure 3). Based on this result, if EDGAR's spatial distribution of N_2O emissions is applied to the urban regions, our result suggests that the actual urban N_2O emissions in California are only marginally higher than CARB's inventory.

3.3. Seasonality in Emissions

We report statewide N_2O emissions for each season because measurements are available for a full annual analysis (June 2013 to May 2014). Figure 5a shows the comparison between the prior state total emission and the posterior total for each season. For all seasons, the posterior emissions are higher than the prior, consistent with the region analysis result in Figure 4. Although the result suggests spring (March–May) emissions may be higher than those of the other seasons, given the large uncertainty range for spring, all seasonal emissions are similar within error. The potentially higher spring emissions can be expected due to the application of agricultural fertilizer during spring and the ensuing conversion of nitrate to N_2O in the soil. This seasonal analysis result agrees with earlier work by Jeong, Zhao, Andrews, Dlugokencky, et al. (2012) that found N_2O emissions for central California varied from 1.6 (±0.6 at 95% confidence) to 2.4 (±0.8) times the EDGAR prior (18.7 Gg N_2O/year). For another comparison, despite using a different spatial model for the prior emissions, Xiang et al. (2013) also found N_2O emissions were larger than the prior emissions during the early summer period.

Our result shows that seasonality in California's N_2O emissions is different from that of the midwestern region. Miller et al. (2012) reported that the estimated N_2O emissions from the midwestern region of the United States during early summer were 3 times those in winter and twice the annual average. However, we note that the emissions in the midwestern region of the United Stated are governed by strong seasonal climate variations in the continental interior and seasonality in agricultural activities. Given the strong correlation between climate, agricultural activities, and emissions in the midwest (Miller et al., 2012), we expect

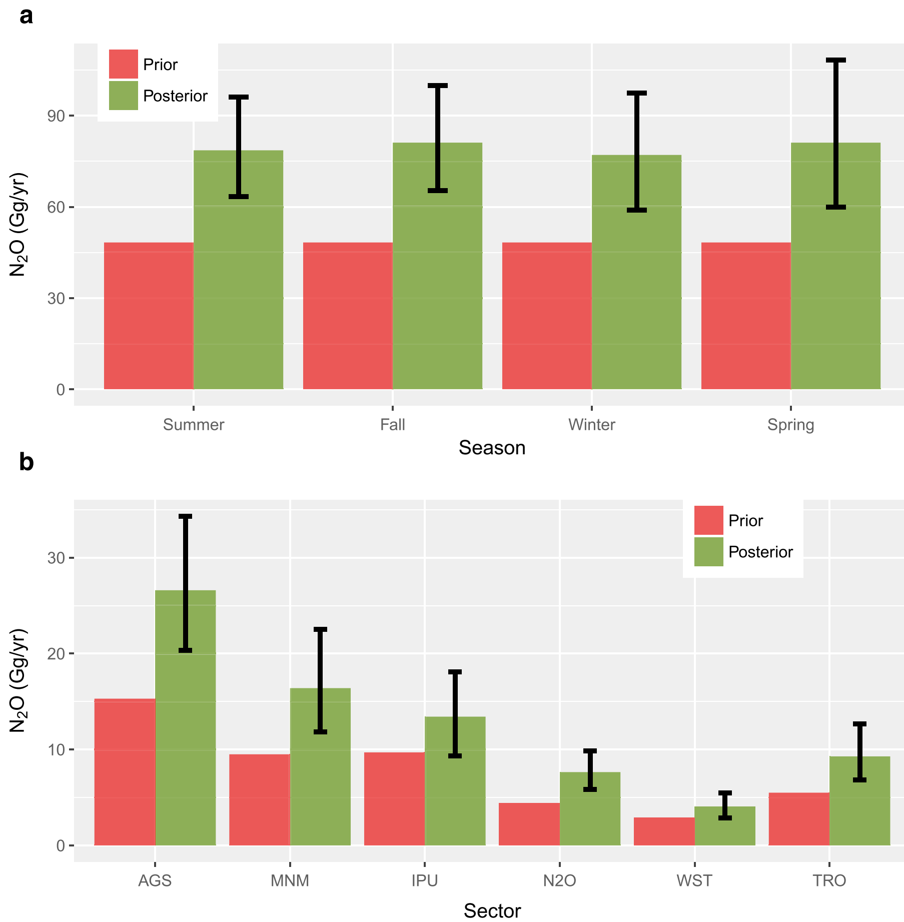

Figure 5. Comparison of anthropogenic prior and posterior N_2O emissions by (a) season and (b) sector (only major sectors are shown). In (b), sectors include agricultural soils (AGS), manure management (MNM), industrial processes and product use (IPU), indirect N_2O emissions from agriculture (N2O), waste (solid and wastewater; WST), and road transportation (TRO).

smaller seasonality in California N_2O emissions due to smaller seasonal temperature variations for the milder California climate leading to more continuous agricultural activities.

3.4. Source Attribution

Source attribution of emissions provides important information in planning mitigation strategies, allowing for prioritizing target sectors. We estimate N2O emissions from different sources assuming the spatial distribution of the CARB-scaled EDGAR prior emission model. Based on this assumption, we scale individual source prior emissions at each pixel or region by the corresponding inferred scaling factor from the HBI analysis to obtain posterior source sector emissions. Figure 5b shows posterior annual emissions for major source sectors estimated from the HBI analysis. We estimate agricultural soil direct N_2O (AGS, synthetic and manure fertilizers and crop residues) emissions to be 20.4–34.3 Gg N_2O/year (at 95% confidence), which are 1.3–2.2 times the prior while indirect N_2O (N2O, nitrogen leaching and runoff) emissions are 5.8–9.9 Gg N_2O/year (1.3–2.2 times the prior). This is consistent with the larger inferred emissions for the Central Valley (see Figure 4) as well as a recent study that attributed a large portion of the increase in global atmospheric N_2O to the use of fertilizers (Park et al., 2012).

Although the agricultural soil sector accounts for the largest portion of the state total N_2O emission, its relative contribution to the total is lower in California compared to that of the United States. While our posterior agricultural soil emissions (both direct and indirect N_2O) are ~43% of the state total posterior emission, U.S. EPA estimates agricultural soils account for ~74% of the U.S. total (1.19 Tg N_2O/year for 2013) N_2O emissions (U.S. EPA, 2015). This relatively low emission ratio of agricultural soil to the total is supported by the region analysis result shown in Figure 4 where the annual posterior emission (across sectors) for the Central Valley, a region dominated by agriculture, was ~50% of the state total. This result suggests that other N_2O source emissions from nonagricultural regions (e.g., SFBA, SoCAB) of California are important. We note that nonagricultural sources (all sectors excluding AGS, N2O, and manure management [MNM]) account for 36% of the total posterior emissions.

The HBI analysis indicates that the second largest sources of N_2O emissions in California are likely MNM and IPU (emissions from chemicals and solvents, e.g., nitric acid, adipic acid, and caprolactam; Janssens-Maenhout et al., 2014). As shown in Figure 5b, the posterior emissions from the two sectors are statistically indistinguishable although the MNM sector yields a larger posterior median emission than that of the IPU sector. Assuming the spatial distribution of our prior model, we estimate the total posterior MNM emission is 1.2–2.4 times higher than the prior, which is consistent with the findings by Owen and Silver (2015) where their estimated N_2O emissions from solid manure piles and anaerobic lagoons alone (included in the MNM sector) were higher than the U.S. EPA estimate by an order of magnitude. We estimate posterior MNM N_2O emissions account for 15–29% of the state total posterior N_2O emission (20% in the prior). Nationally, U.S. EPA estimates the manure accounts for only 5% of the U.S. total N_2O in 2013 (U.S. EPA, 2015). However, Guha et al. (2015) report that dairy and other livestock contribute 60–70% of daily N_2O enhancements near Bakersfield (Region 8 in this study) during May–June 2010, suggesting that the contribution of MNM in California is likely larger than the national average, in agreement with our posterior estimates and the CARB inventory.

4. Conclusions

We report the first annual analysis of anthropogenic N_2O emissions using atmospheric observations from six sites across California. We find that state annual anthropogenic emissions are 1.5–2.5 times higher (at 95% confidence) than that (41 Gg N_2O/year in 2014) of a recent state inventory (CARB, 2016). This estimate for N_2O amounts to 4–7% of the total GHG emissions for California (442 Tg CO_2eq in 2014; CARB, 2016). This result suggests that the total N_2O emission is not only underestimated in the state inventory but also controlling emissions of N_2O is a necessary component to meet California's 40% and 80% GHG reduction goals for 2030 and 2050, respectively. Using a measurement network across California, for the first time, an annual budget for California's major N_2O-emitting regions have been quantified constraining N_2O emissions from California's two major urban regions and the Central Valley. This result demonstrates that our approach can be a useful tool to evaluate the implementation of California's climate policies accounting for long-term spatial and temporal changes in N_2O emissions. Our study results reinforce the understanding that agricultural activities are a significant source of anthropogenic N_2O emissions in California (Jeong, Zhao, Andrews, Dlugokencky, et al., 2012; Xiang et al., 2013). Our results also indicate that seasonal variations in California's N_2O emissions are small compared to that of the midwestern region of the United States. However, to further characterize seasonal and interannual variability of emissions that are affected by weather patterns, fertilizer use, and crop production (U.S. EPA, 2015), more measurements with longer temporal and denser spatial coverage are required. In this study, we have shown that the added measurement sites to the N_2O network in conjunction with a robust inverse modeling system significantly reduced the posterior uncertainty estimates over previous studies. In the future, a combination of improved prior emission and meteorological models, expanded multigas measurements, and inverse model analyses will further reduce uncertainty in California's N_2O emissions.

Acknowledgments
We thank Dave Field, Dave Bush, Edward Wahl, Ken Reichl, Toby Walpert, and particularly Jon Kofler for assistance with measurements at WGC, Ying-Kuang Hsu, Bart Croes, Jorn Herner, Abhilash Vijayan, Matthias Falk, Richard Bode, Anny Huang, Jessica Charrier, Kevin Eslinger, Larry Hunstaker, Ken Stroud, Mac McDougall, Jim Nyarady, and others for sharing CARB emissions information and providing valuable review comments. This study was in part supported by the CARB Research Division (CARB contract 11-306) under U.S. Department of Energy contract DE-AC02-05CH11231. The statements and conclusions in this paper are those of the authors and not necessarily those of the CARB. The mention of commercial products, their source, or their use in connection with material reported herein is not to be construed as actual or implied endorsement of such products. Also, this document was prepared as an account of work sponsored by the U.S. Government. While this document is believed to contain correct information, neither the U.S. Government nor any agency thereof, nor The Regents of the University of California, nor any of their employees, makes any warranty, express or implied, or assumes any legal responsibility for the accuracy, completeness, or usefulness of any information, apparatus, product, or process disclosed, or represents that its use would not infringe privately owned rights. Reference herein to any specific commercial product, process, or service by its trade name, trademark, manufacturer, or otherwise does not necessarily constitute or imply its endorsement, recommendation, or favoring by the U.S. Government or any agency thereof, or The Regents of the University of California. The views and opinions of authors expressed herein do not necessarily state or reflect those of the United States Government or any agency thereof, or The Regents of the University of California. Ernest Orlando Lawrence Berkeley National Laboratory is an equal opportunity employer. STR and WGC measurement data are available through https://www.esrl.noaa.gov/gmd/ccgg/flask.php, and data for CARB sites are available at https://www.arb.ca.gov/aqmis2/res/aqdselect.php?tab=hourly. The data used in the inversion are shown in supporting information Figure S8. The EDGAR and CARB prior emissions are available at http://edgar.jrc.ec.europa.eu and https://www.arb.ca.gov/cc/inventory/inventory.htm, respectively.

References

Bagley, J. E., Jeong, S., Cui, X., Newman, S., Zhang, J., Priest, C., et al. (2017). Assessment of an atmospheric transport model for annual inverse estimates of California greenhouse gas emissions. *Journal of Geophysical Research: Atmospheres*, *122*, 1901–1918. https://doi.org/10.1002/2016JD025361

Bouwman, A. F., van der Hoek, K. W., & Olivier, J. G. J. (1995). Uncertainties in the global source distribution of nitrous oxide. *Journal of Geophysical Research*, *100*, 2785–2800. https://doi.org/10.1029/94JD02946

California Air Resources Board (2014). California greenhouse gas emissions inventory, *California Air Resources Board Staff Report*. Retrieved in January 2015 from http://www.arb.ca.gov/cc/inventory/inventory.htm, version March 2014.

California Air Resources Board (2016). California greenhouse gas emissions inventory. *California Air Resources Board Staff Report*. Retrieved in September 2016 from http://www.arb.ca.gov/cc/inventory/inventory.htm

Chen, F., & Dudhia, J. (2001). Coupling an advanced land surface hydrology model with the Penn State NCAR MM5 modeling system. Part 1: Model implementation and sensitivity. *Monthly Weather Review*, *129*(4), 569–585. https://doi.org/10.1175/1520-0493(2001)129<0569:CAALSH>2.0.CO;2

Cui, Y. Y., Brioude, J., Angevine, W. M., Peischl, J., McKeen, S. A., Kim, S. W., et al. (2017). Top-down estimate of methane emissions in California using a mesoscale inverse modeling technique: The San Joaquin Valley. *Journal of Geophysical Research: Atmospheres*, *122*, 3686–3699. https://doi.org/10.1002/2016JD026398

Fischer, M. L., Parazoo, N., Brophy, K., Cui, X., Jeong, S., Liu, J., et al. (2017). Simulating estimation of California fossil fuel and biosphere carbon dioxide exchanges combining in situ tower and satellite column observations. *Journal of Geophysical Research: Atmospheres*, *122*, 3653–3671. https://doi.org/10.1002/2016JD025617

Ganesan, A. L., Rigby, M., Zammit-Mangion, A., Manning, A. J., Prinn, R. G., Fraser, P. J., et al. (2014). Characterization of uncertainties in atmospheric trace gas inversions using hierarchical Bayesian methods. *Atmospheric Chemistry and Physics*, *14*(8), 3855–3864. https://doi.org/10.5194/acp-14-3855-2014

Gelman, A., Carlin, J. B., Stern, H. S., Dunson, D. B., Vehtari, A., & Rubin, D. B. (2014). *Bayesian data analysis* (3rd ed.). Boca Raton, FL: Chapman & Hall/CRC.

Gelman, A., & Hill, J. (2007). *Data analysis using regression and multilevel/hierarchical models*. New York: Cambridge University Press.

Gelman, A., & Rubin, D. B. (1992). Inference from iterative simulation using multiple sequences. *Statistical Science*, *7*(4), 457–472. https://doi.org/10.1214/ss/1177011136

Guha, A., Gentner, D. R., Weber, R. J., Provencal, R., Gardner, A., & Goldstein, A. H. (2015). Source apportionment of methane and nitrous oxide in California's San Joaquin Valley at CalNex 2010 via positive matrix factorization. *Atmospheric Chemistry and Physics*, *15*(20), 12,043–12,063. https://doi.org/10.5194/acp-15-12043-2015

Hall, B. D., Dutton, G. S., & Elkins, J. W. (2007). The NOAA nitrous oxide standard scale for atmospheric observations. *Journal of Geophysical Research*, *112*, D09305. https://doi.org/10.1029/2006JD007954

Hofmann, D. J., Butler, J. H., Dlugokencky, E. J., Elkins, J. W., Masarie, K., Montzka, S. A., & Tans, P. (2006). The role of carbon dioxide in climate forcing from 1979–2004: Introduction of the annual greenhouse gas index. *Tellus B*, *58B*, 614–619.

Hong, S., Noh, Y., & Dudhia, J. (2006). A new vertical diffusion package with an explicit treatment of entrainment processes. *Monthly Weather Review*, *134*(9), 2318–2341. https://doi.org/10.1175/MWR3199.1

Janjić, Z. I. (1990). The step-mountain coordinate: Physical package. *Monthly Weather Review*, *118*(7), 1429–1443. https://doi.org/10.1175/1520-0493(1990)118<1429:TSMCPP>2.0.CO;2

Janssens-Maenhout, G., Guizzardi, D., Bergamaschi, P., & Muntean, M. (2014). On the CH_4 and N_2O emission inventory compiled by EDGAR and improved with EPRTR data for the INGOS project (JRC-IES-H02-EDGAR). European Commission Joint Research Centre. Retrieved in October 2015 from http://edgar.jrc.ec.europa.eu/ingos/JRC-INGOS-report.pdf

Jeong, S., Cui, X., Blake, D. R., Miller, B., Montzka, S. A., Andrews, A., et al. (2017). Estimating methane emissions from biological and fossil-fuel sources in the San Francisco Bay Area. *Geophysical Research Letters*, *44*, 486–495. https://doi.org/10.1002/2016GL071794

Jeong, S., Hsu, Y.-K., Andrews, A. E., Bianco, L., Vaca, P., Wilczak, J. M., & Fischer, M. L. (2013). A multitower measurement network estimate of California's methane emissions. *Journal of Geophysical Research: Atmospheres*, *118*(19), 11,339–11,351. https://doi.org/10.1002/jgrd.50854

Jeong, S., Newman, S., Zhang, J., Andrews, A. E., Bianco, L., Bagley, J., et al. (2016). Estimating methane emissions in California's urban and rural regions using multitower observations. *Journal of Geophysical Research: Atmospheres*, *121*, 13,031–13,049. https://doi.org/10.1002/2016JD025404

Jeong, S., Zhao, C., Andrews, A. E., Bianco, L., Wilczak, J. M., & Fischer, M. L. (2012). Seasonal variation of CH_4 emissions from central California. *Journal of Geophysical Research*, *117*, D11306. https://doi.org/10.1029/2011JD016896

Jeong, S., Zhao, C., Andrews, A. E., Dlugokencky, E. J., Sweeney, C., Bianco, L., et al. (2012). Seasonal variations in N_2O emissions from central California. *Geophysical Research Letters*, *39*, L16805. https://doi.org/10.1029/2012GL052307

Jiménez, P. A., & Dudhia, J. (2012). Improving the representation of resolved and unresolved topographic effects on surface wind in the WRF model. *Journal of Applied Meteorology and Climatology*, *51*(2), 300–316. https://doi.org/10.1175/JAMC-D-11-084.1

Johnson, M. S., Xi, X., Jeong, S., Yates, E. L., Iraci, L. T., Tanaka, T., et al. (2016). Investigating seasonal methane emissions in northern California using airborne measurements and inverse modeling. *Journal of Geophysical Research: Atmospheres*, *121*, 13,753–13,767. https://doi.org/10.1002/2016JD025157

Kass, R. E., Carlin, B. P., Gelman, A., & Neal, R. M. (1998). Markov Chain Monte Carlo in practice: A roundtable discussion. *The American Statistician*, *52*(2), 93–100. https://doi.org/10.1080/00031305.1998.10480547

Korner-Nievergelt, F., Roth, T., von Felten, S., Guélat, J., Almasi, B., & Korner-Nievergelt, P. (2015). *Bayesian data analysis in ecology using linear models with R, BUGS, and Stan: Including comparisons to frequentist statistics*. New York: Elsevier Science.

Kort, E. A., Eluszkiewicz, J., Stephens, B. B., Miller, J. B., Gerbig, C., Nehrkorn, T., et al. (2008). Emissions of CH_4 and N_2O over the United States and Canada based on a receptor-oriented modeling framework and COBRA-NA atmospheric observations. *Geophysical Research Letters*, *35*, L18808. https://doi.org/10.1029/2008GL034031

Kruschke, J. K. (2015). *Doing Bayesian data analysis* (2nd ed.). New York: Academic Press.

Legislative Information (2006). Assembly bill AB32, official California legislative information, 27 September. Retrieved in May 2017 from http://www.leginfo.ca.gov/pub/05-06/bill/asm/ab_0001-0050/ab_32_bill_20060927_chaptered.html

Legislative Information (2016). SB-32 California global warming solutions act of 2006: Emissions limit. Retrieved in May 2017 from https://leginfo.legislature.ca.gov/faces/billNavClient.xhtml?bill_id=201520160SB32

Lin, J. C., Gerbig, C., Wofsy, S. C., Andrews, A. E., Daube, B. C., Davis, K. J., & Grainger, C. A. (2003). A near-field tool for simulating the upstream influence of atmospheric observations: The Stochastic Time-Inverted Lagrangian Transport (STILT) model. *Journal of Geophysical Research*, *108*(D16), 4493. https://doi.org/10.1029/2002JD003161

Mellor, G. L., & Yamada, T. (1982). Development of a turbulence closure model for geophysical fluid problems. *Reviews of Geophysics and Space Physics*, *20*(4), 851–875. https://doi.org/10.1029/RG020i004p00851

Mesinger, F., DiMego, G., Kalnay, E., Mitchell, K., Shafran, P. C., Ebisuzaki, W., et al. (2006). North American regional reanalysis. *Bulletin of the American Meteorological Society*, *87*(3), 343–360. https://doi.org/10.1175/BAMS-87-3-343

Michalak, A. M. (2008). A Gibbs sampler for inequality-constrained geostatistical interpolation and inverse modeling. *Water Resources Research*, *44*, W09437. https://doi.org/10.1029/2007WR006645

Miller, S. M., Kort, E. A., Hirsch, A. I., Dlugokencky, E. J., Andrews, A. E., Xu, X., et al. (2012). Regional sources of nitrous oxide over the United States: Seasonal variation and spatial distribution. *Journal of Geophysical Research*, *117*, D06310. https://doi.org/10.1029/2011JD016951

Miller, S. M., Michalak, A. M., & Levi, P. J. (2014). Atmospheric inverse modeling with known physical bounds: An example from trace gas emissions. *Geoscientific Model Development*, *7*(1), 303–315. https://doi.org/10.5194/gmd-7-303-2014

Montzka, S. A., Dlugokencky, E. J., & Butler, J. H. (2011). Non-CO_2 greenhouse gases and climate change. *Nature*, *476*(7358), 43–50. https://doi.org/10.1038/nature10322

Myhre, G., Shindell, D., Bréon, F.-M., Collins, W., Fuglestvedt, J., Huang, J., et al. (2013). Anthropogenic and natural radiative forcing. In T. F. Stocker, et al. (Eds.), *Climate change 2013: The physical science basis. Contribution of working group I to the fifth assessment report of the Intergovernmental Panel on Climate Change* (Chapter 8, pp. 659–740). Cambridge, United Kingdom and New York, NY: Cambridge University Press.

Nakanishi, M., & Niino, H. (2006). An improved Mellor Yamada level-3 model: Its numerical stability and application to a regional prediction of advection fog. *Boundary-Layer Meteorology*, *119*(2), 397–407. https://doi.org/10.1007/s10546-005-9030-8

Nehrkorn, T., Eluszkiewicz, J., Wofsy, S. C., Lin, J. C., Gerbig, C., Longo, M., & Freitas, S. (2010). Coupled weather research and forecasting—Stochastic time-inverted lagrangian transport (WRF-STILT) model. *Meteorology and Atmospheric Physics*, *107*(1-2), 51–64. https://doi.org/10.1007/s00703-010-0068-x

Newman, S., Jeong, S., Fischer, M. L., Xu, X., Haman, C. L., Lefer, B., et al. (2013). Diurnal tracking of anthropogenic CO_2 emissions in the Los Angeles basin megacity during spring 2010. *Atmospheric Chemistry and Physics*, *13*(8), 4359–4372. https://doi.org/10.5194/acp-13-4359-2013

Office of Governor (2005). California's Executive Order (EO) S-3-05. Retrieved in May 2017 from https://www.gov.ca.gov/2014/07/21/news18610/

Owen, J., & Silver, W. L. (2015). Greenhouse gas emissions from dairy manure management: A review of field-based studies. *Global Change Biology*, *21*(2), 550–565. https://doi.org/10.1111/gcb.12687

Park, S., Croteau, P., Boering, K. A., Etheridge, D. M., Ferretti, D., Fraser, P. J., et al. (2012). Trends and seasonal cycles in the isotopic composition of nitrous oxide since 1940. *Nature Geoscience*, *5*(4), 261–265. https://doi.org/10.1038/NGEO1421

Plummer, M. (2003). JAGS: A program for analysis of Bayesian graphical models using Gibbs sampling. Paper presented at the 3rd International Workshop on Distributed Statistical Computing (DSC 2003), March 20–22, Vienna, Austria.

Rasmussen, C. E., & Williams, C. K. I. (2006). *Gaussian processes for machine learning*. Cambridge, Massachusetts: MIT Press.

Ravishankara, A. R., Daniel, J. S., & Portmann, R. W. (2009). Nitrous oxide (N_2O): The dominant ozone-depleting substance emitted in the 21st century. *Science*, *325*, 123–125.

Skamarock, W. C., Klemp, J. B., Dudhia, J., Gill, D. O., Barker, D. M., Huang, X. Z., et al. (2008). *A description of the advanced research WRF version 3 (Technical Note 475+STR)*. Boulder, Colorado: Mesoscale and Microscale Meteorology Division, NCAR.

Solomon, S., et al. (2007). Technical summary, In: *Climate change 2007: The physical science basis. contribution of working group I to the fourth assessment report of the Intergovernmental Panel on Climate Change* (pp. 19–91), Solomon, S., Qin, D., Manning, M., Chen, Z., Marquis, M., Averyt, K. B., Tignor, M. & Miller, H. L. (eds.), Cambridge University Press, Cambridge, United Kingdom and New York, NY.

U.S. EPA (2015). Inventory of U.S. greenhouse gas emissions and sinks: 1990—2013 (430-R-15-004). Washington D.C.: Environmental Protection Agency. Retrieved in September 2015 from http://www.epa.gov/climatechange/Downloads/ghgemissions/US-GHG-Inventory-2015-Main-Text.pdf

Wecht, K. J., Jacob, D. J., Sulprizio, M. P., Santoni, G. W., Wofsy, S. C., Parker, R., et al. (2014). Spatially resolving methane emissions in California: Constraints from the CalNex aircraft campaign and from present (GOSAT, TES) and future (TROPOMI, geostationary) satellite observations. *Atmospheric Chemistry and Physics*, *14*(15), 8173–8184. https://doi.org/10.5194/acp-14-8173-2014

Xiang, B., Miller, S. M., Kort, E. A., Santoni, G. W., Daube, B. C., Commane, R., et al. (2013). Nitrous oxide (N_2O) emissions from California based on 2010 CalNex airborne measurements. *Journal of Geophysical Research: Atmospheres*, *118*, 2809–2820. https://doi.org/10.1002/jgrd.50189

Zhao, C., Andrews, A. E., Bianco, L., Eluszkiewicz, J., Hirsch, A., MacDonald, C., et al. (2009). Atmospheric inverse estimates of methane emissions from Central California. *Journal of Geophysical Research*, *114*, D16302. https://doi.org/10.1029/2008JD011671